Electronic Supplementary Material (ESI) for Journal of Materials Chemistry A.

Supporting Information

Seawater desalination derived entirely from ocean biomass

Xiaojie Liu,[a] Yanpei Tian,[a] Yanzi Wu,[a] Andrew Caratenuto,[a] Fangqi Chen,[a] Shuang Cui,[b] Joseph A DeGiorgis,[c,d] Yinsheng Wan,[d] and Yi Zheng*[a]

[a]Department of Mechanical and Industrial Engineering, Northeastern University, Boston, MA 02115, USA.

[b]National Renewable Energy Laboratory, Golden, CO 80401, USA.

[c]Whitman Center, Marine Biological Laboratory, Woods Hole, MA 02543, USA.

[d]Department of Biology, Providence College, Providence, RI 02918, USA.

*e-mail: y.zheng@northeastern.edu

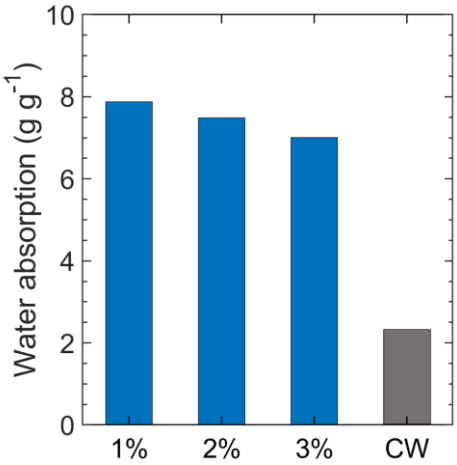

Figure S1. Water absorption rate of the CI/CS hydrogels with different chitosan concentration in comparison with the carbonized wood (CW). The CW used here are fabricated by carbonizing the balsa wood (3 cm x 3 cm x 0.5 cm) at 800°C under a protective environment of argon.

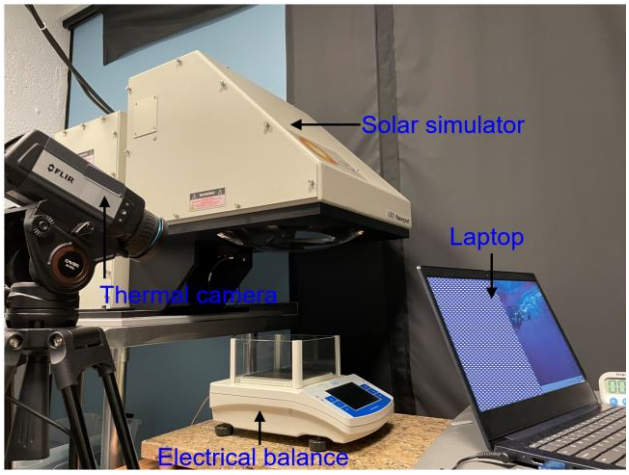

Figure S2. Photograph of the experimental setup for desalination tests.

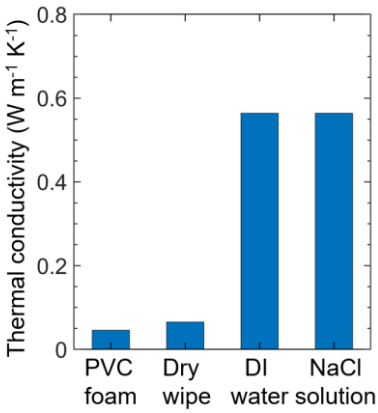

Figure S3. Thermal conductivities of PVC foam, dry cotton wipe, cotton wipe soaked in DI water, and cotton wipe soaked in 3.5 wt% NaCl solution, respectively. The PVC foam we used in this work in the thickness of 7 mm has a low thermal conductivity of 0.041 W m^{-1} K^{-1}, serving as a thermal insulation layer in the evaporation device to reduce the downward. The dry cotton wipe has a thermal conductivity of 0.065 W m^{-1} K^{-1}, which is a little higher than that of the PVC foam. The intrinsic low thermal conductivity of the cotton wipe helps to restrict the generated heat to bulk water. After soaking the cotton wipe into DI water and 3.5 wt% NaCl solution, respectively, the thermal conductivity keeps unchanged remaining at 0.564 W m^{-1} K^{-1}.

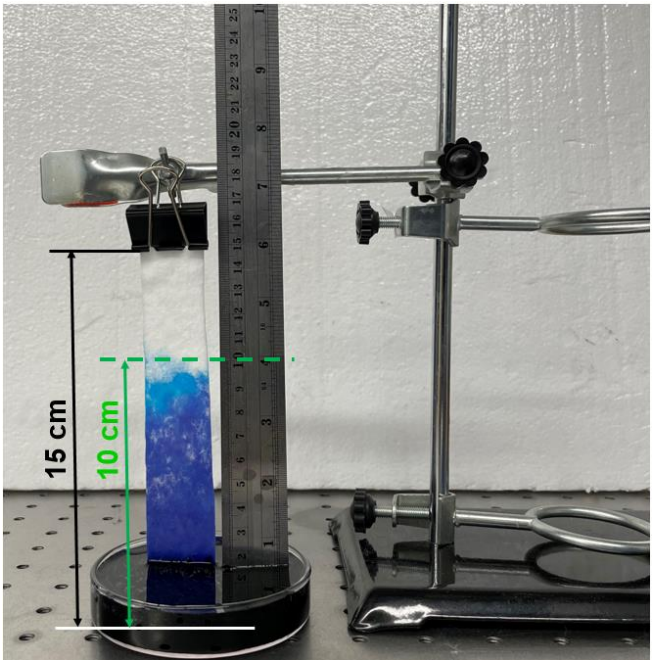

Figure S4. Photograph of water absorption ability of cotton wipe strip. The 15 cm in length and 3 cm in width cotton wipe strip is fixed vertically using a binder clip. One end of the strip is soaked in water with blue dye. Due to the porous structure and the super hydrophilicity of the cotton wipe, water can be effectively transported to a height of 10 cm from the bottom (green dash line).

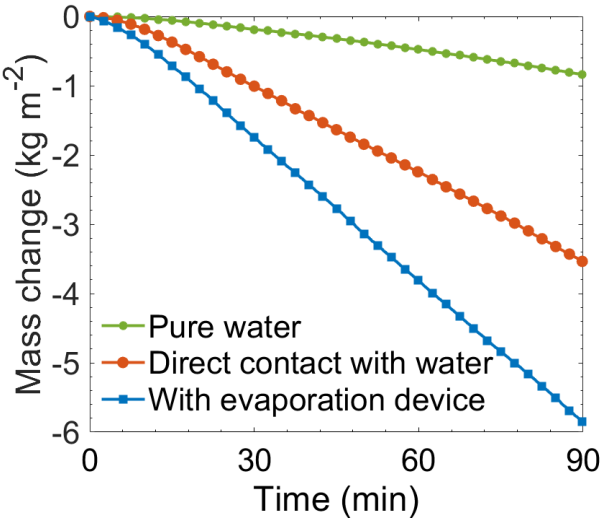

Figure S5. Mass changes of water for the CI/CS evaporator with the different water supply methods in comparison to pure water as a control test for 90 min.

Supplementary note S1:

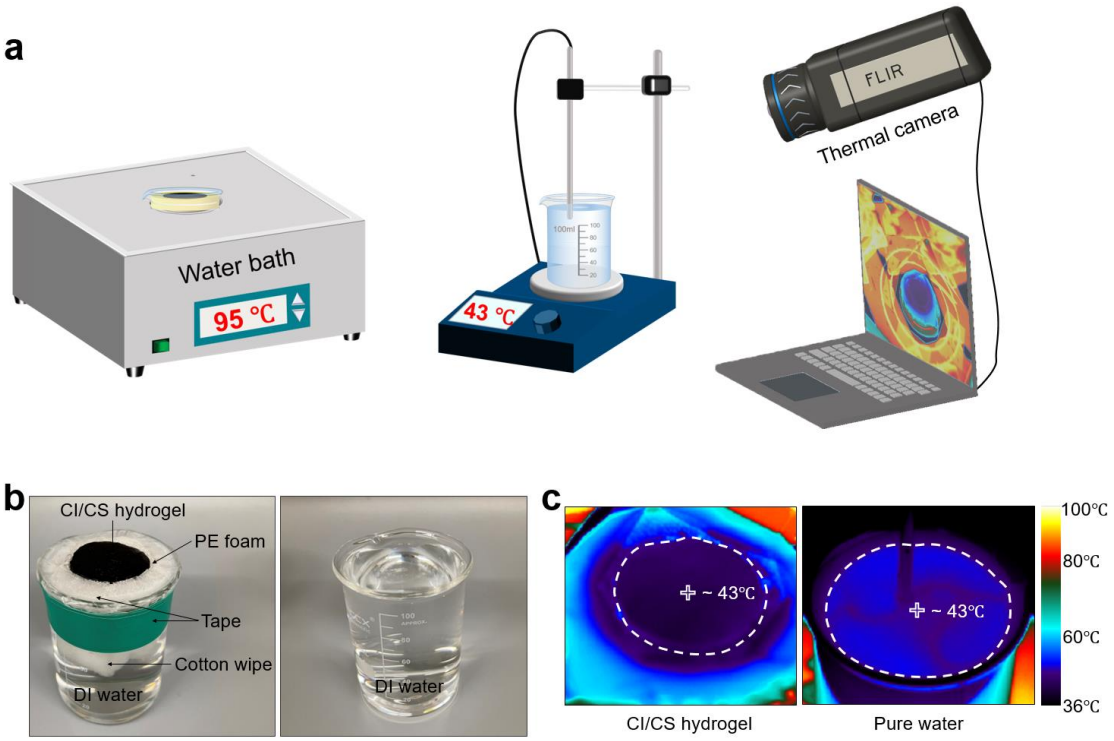

Figure S6. (a) The experimental setup for calculating the equivalent evaporation enthalpy when the evaporation surface temperatures of the CI/CS hydrogel evaporator and pure water are kept at 43℃. (b) Photographs of the CI/CS hydrogel evaporation device and pure water used under dark. (c) The infrared images showing the temperature distribution of surfaces for the CI/CS hydrogel evaporator and pure water after reaching the stable state.

To evaluate the equivalent evaporation enthalpy of water in the CI/CS hydrogel evaporator at its operating temperature (43℃), the dark environment experiment during which the evaporation surface temperature of the CI/CS hydrogel evaporator and the pure water are both 43℃ in a dark room (21℃) is conducted.

Figure S6a shows the experimental setup of dark environment test for calculating the equivalent evaporation enthalpy of CI/CS hydrogel. To keep the evaporation surface of the CI/CS hydrogel evaporator and pure water at the operating temperature of evaporator (43℃), the evaporation device of the CI/CS hydrogel evaporator is placed into a water bath stabilized at 95℃ to make the surface temperature of the CI/CS evaporator up to 43℃. While the temperature of the pure water surface is kept at 43℃ using a temperature-controlled hot plate. These surface temperatures of the CI/CS hydrogel evaporator and pure water were monitored by a thermal camera. The device with the CI/CS hydrogel evaporator is shown in Figure S6b and the outer surface of the beaker is surrounded by tapes to reduce the gap between the beaker and the holding port of the water bath. After the surface temperatures of the CI/CS hydrogel and the pure water are heated and stabilized at 43℃ for 15 min (Figure S6c), the initial masses of the CI/CS hydrogel evaporation device and the pure water with a beaker are weighted, and put them back to the water bath and hot plate, respectively, to carry out the dark environment. After more than 4 hours, the final masses are recorded. This experiment is repeated 2 times and the average evaporation rates of water with CI/CS hydrogel evaporator and the pure water under the dark environment are calculated, as listed in Table S1 below.

Table S1. The average evaporation rates of water with CI/CS hydrogel evaporation device and pure water for different dark environment tests.

Test	Evaporation rate of pure water ($kg\ m^{-2}\ h^{-1}$)	Evaporation rate of CI/CS evaporator device ($kg\ m^{-2}\ h^{-1}$)	Evaporation rate ratio (water/CI/CS evaporator)
1	0.982	3.685	0.267
2	1.000	3.638	0.276

The calculation of the equivalent water evaporation enthalpy is listed below.

The photothermal efficiency η_{pt} of an absorber can be calculated using the equation $\eta_{pt} = \dot{m}h_{equ}/Q_s$, where $\dot{m}$ is water evaporation rate, $h_{equ}$is the equivalent enthalpy of the water in the CI/CS hydrogel at the operating temperature under sunlight illumination, and Q_s refers to the power density of the incoming light illumination.

The equivalent enthalpy h_{equ} can be estimated using the following formula:

$$h_{equ} = \frac{\dot{m}_{water}}{\dot{m}_{CI/CS}} h_{fg}^{w}$$

where $\dot{m}_{water}$ is the evaporation rate of pure water, $\dot{m}_{CI/CS}$ is evaporation rate of the CI/CS hydrogel evaporator, and h_{fg}^{w} is temperature-dependent vaporization enthalpy of pure water. Note that $\dot{m}_{water}$ and $\dot{m}_{CI/CS}$ are the evaporation rates we obtain in the dark environment experiments. The water evaporation enthalpy of pure water at 43℃ is 2398.8 kJ kg^{-1}. Accordingly, the equivalent vaporization enthalpy h_{equ} is

$$h_{equ} = 0.267 \times 2398.8 = 640.480\ \text{kJ kg}^{-1} \quad \text{for test 1}$$

$$h_{equ} = 0.276 \times 2398.8 = 662.069\ \text{kJ kg}^{-1} \quad \text{for test 2}$$

Therefore, the corresponding photothermal efficiency η_{pt} for test 1 is calculated to be 72.94% and for test 2 is 75.40%.

Supplementary note S2:

The energy loss of the CI/CS hydrogel evaporator consists of radiative heat loss (P_{rad}) form the top evaporation surface, convective heat loss (P_{conv}) between the surrounding air and top evaporation surface, and conductive heat loss (P_{cond}) between the evaporator and the bulk water.

(1) Radiative heat loss (P_{rad}):

The radiative heat loss can be calculated by the Planck's radiation law.

$P_{rad} = \varepsilon\sigma(T_{evap}^4 - T_{air}^4)$, where ε means the overall emissivity of the top evaporation surface of CI/CS hydrogel evaporator when it is in working mode. It is calculated to be 0.96 and its emissivity spectrum is shown in Figure S7. σ represents the Stefan-Boltzmann constant (5.67×10^{-8} W m^{-2} K^{-4}). T_{evap} and T_{air} are the stable temperature of the evaporator (316 K) and surrounding air (305 K), respectively. Therefore, the radiative heat loss is estimated to be ~ 71.7 W m^{-2} and the radiative heat loss rate is about 7.17%.

(2) Convective heat loss (P_{conv}):

$P_{conv} = h(T_{evap} - T_{air})$, where h represents the convective heat transfer coefficient (~ 5 W m^{-2} K^{-1}). Therefore, the convective heat loss is about 55 W m^{-2}, and the convective heat loss rate is about 5.5%.

(3) Conductive heat loss (P_{cond}):

$P_{cond} = Cm\Delta T/(A \times t)$, where C denotes the specific heat capacity of water (4,200 J K^{-1} kg), m is the weight of the bulk water (72 g), and ΔT is the temperature increase of the bulk water when its temperature stabilizes. Here, the temperature of the bulk water increase from 20.3 to 21.1°C within 90 min. A is the surface area of the evaporator (420 mm^2). t is the experimental time for one evaporation rate test (90 min). Therefore, the conduction heat loss is 106.7W m^{-2}, and its rate is 10.7%.

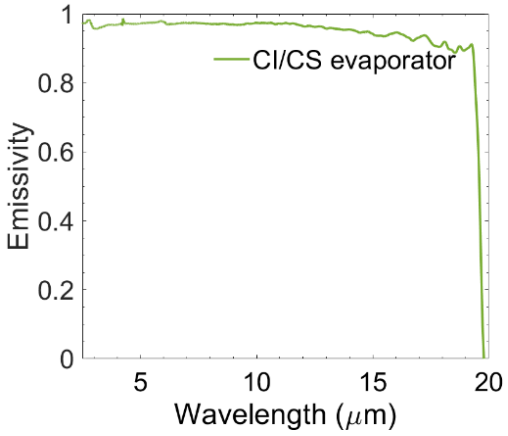

Figure S7. The emissivity spectra of the top surface of the CI/CS hydrogel evaporator.

Supplementary note S3:

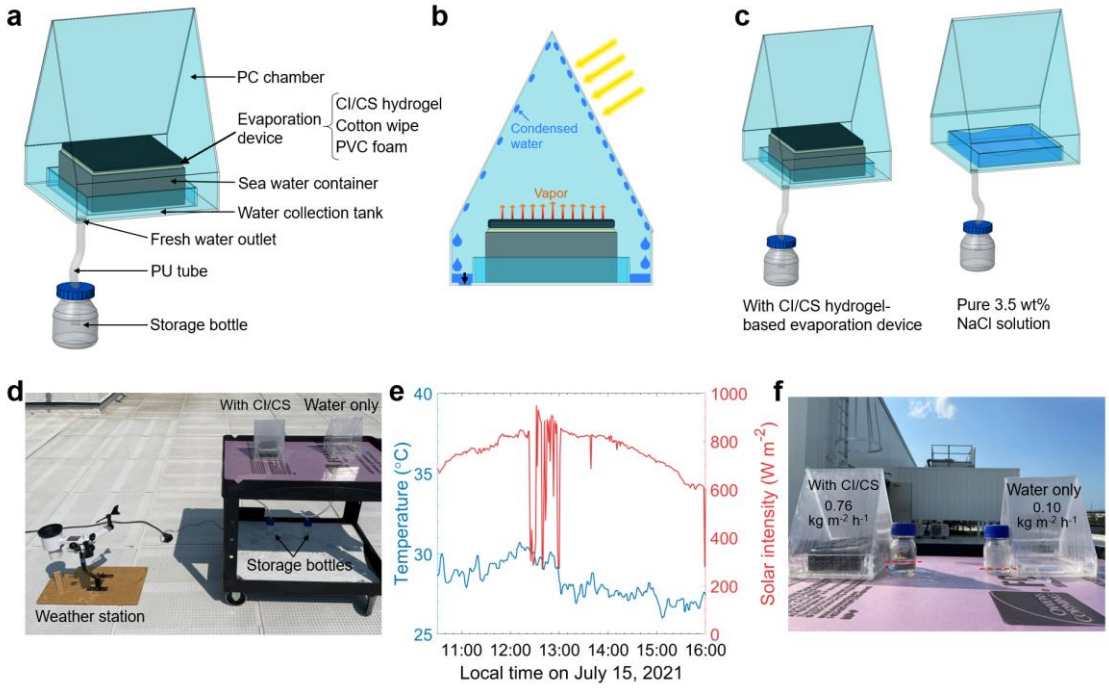

Figure S8. Outdoor solar-driven desalination test. (a) Three-dimensional (3D) model of the solar desalination system based on the CI/CS hydrogel evaporator. (b) Schematic illustrating the mechanism of water evaporation and freshwater collection. (c) 3D model of solar-driven desalination system with CI/CS hydrogel evaporator (left) and the control group without hydrogel evaporator (right). (d) Photograph of the solar-driven desalination chambers which are placed on a utility cart (right) and the weather station (left) for recording the data of solar irradiance intensity and ambient temperature. (e) Ambient temperature (solid blue curve) and solar intensity (solid red curve) variations during the outdoor desalination test. (f) Photograph showing the contrast of water collection rate between the CI/CS hydrogel desalination system and the control group with only 3.5 wt% NaCl solution.

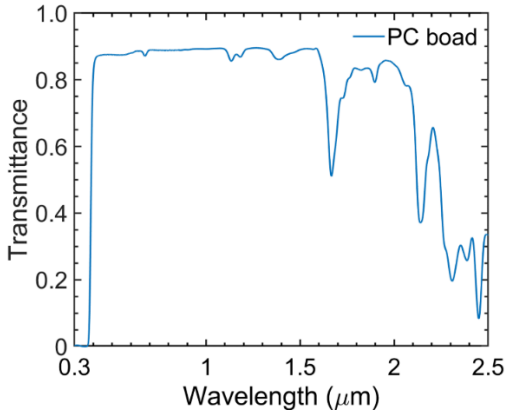

Figure S9. Transmittance spectrum of the 0.8 mm PC board over the solar wavelengths.

The outdoor solar desalination experiment was tested on the roof of Snell Engineering Center at Northeastern University, Boston, MA, USA on July 15, 2021. The solar desalination system is composed of a sealed condensation chamber and a CI/CS evaporation device with a large area of the absorber (9 cm × 9 cm) inside (Figure S8a). The condensation chamber covers on top of the CI/CS hydrogel evaporation device to capture the evaporated vapor. Besides, the chamber is made of polycarbonate (PC) board with a thickness of 0.8 mm and an overall transmittance of 83% (Figure S9) for the solar wavelengths (0.3 - 2.5 μm). The PC board is transparent in the solar spectrum to allow the solar irradiance to reach the CI/CS hydrogel evaporator. The structure of the evaporation device consists of the CI/CS hydrogel as an evaporator, cotton wipe as the water transportation path and salt rejection path, and the PVC foam as a thermal barrier layer. The evaporation device floats on a water container (10 cm × 10 cm × 4 cm) which is filled with the 3.5 wt% NaCl solution. The generated freshwater flows to the water storage bottle through a polyurethane (PU) tube. The generated water vapor from the CI/CS hydrogel evaporator condensates on the inner wall of the PC board, and then, the condensed water droplets flow downward along the wall to the water collection tank and finally to the water storage bottle (Figure S8b).

The experimental group encapsulated the CI/CS hydrogel evaporation device inside, while only the 3.5 wt% NaCl solution is stored inside the water container (11 cm × 11 cm × 2 cm) as a control group without any photothermal materials (Figure S8c). Both the experimental and the control group of the solar desalination system are placed on the polystyrene (PS) form between the bottom of the two prototypes and the utility cart (Figure S8d). The PS foam has a low thermal conductivity of 0.03 W m^{-1} K^{-1} and it can effectively block the heat transfer between the PC prototype chambers and the black utility cart since the cart can be heated up to a high temperature under sunlight in the summer. Those two water storage bottles are placed in the shade of the utility cart to reduce the water re-evaporation in a high-temperature environment. The weather station records the data of the solar intensity and ambient temperature, as shown in Figure S8e. The average ambient temperature and solar intensity are 28.3℃ and 744.7 W m^{-2}, respectively, during the experimental period from 10:30 to 16:00. At the end of the outdoor experiment, 33.7g of water is collected in the storage bottle from the prototype with CI/CS hydrogel evaporator, while the control group only collects 6.4g of water (Figure S8f). The average freshwater collection rate of the CI/CS evaporation device group is 0.76 kg m^{-2} h^{-1}, while the control group is only 0.10 kg m^{-2} h^{-1}. It is worth noting that the weight of the collected freshwater is less than that of the condensed water. The obvious difference between the experimental and control group validate the good performance of the CI/CS hydrogel evaporation device.

Table S2. The weights of CI/CS porous structures with different chitosan concentrations in dry and hydrated states.

Chitosan concentration	1%	2%	3%
W_{i_1}	0.3939	0.4198	0.7685
W_{i_2}	0.3946	0.4201	0.768
W_{i_3}	0.3938	0.4221	0.7683
W_i	0.3941	0.4206	0.7682
W_{f_1}	3.4239	3.4959	6.2501
W_{f_2}	3.5366	3.6262	6.0405
W_{f_3}	3.531	3.5816	6.1678
W_f	3.4971	3.5679	6.1528
W_w	3.1030	3.1472	5.3845
Ratio	7.8738	7.4815	7.0086

The water absorption ratio of CI/CS hydrogel can be calculated by the following formula: $R = (W_f - W_i)/W_i$. Where, R is the water absorption ratio of CI/CS porous structure. W_i is the average initial weight (dry state), and W_f is the average final weight (hydrated state) of CI/CS hydrogel. $W_w = W_f - W_i$ is the water mass absorbed of the hydrogel. Every sample was weighed three times for both dry and hydrated states with the values of W_{i_n} and W_{f_n} (n=1,2,3). All weights are in grams.

Table S3. Steam generation performance of CI/CS-based evaporation device compared with other biomass-based works.

Evaporation rate ($kg\ m^{-2}\ h^{-1}$)	Biomass materials	Reference
1.78	Chitosan and carbonized pomelo peel	Ref. [1]
1.7	Chitosan	Ref. [2]
1.62	Sodium alginate	Ref. [3]
1.3	Enteromorpha prolifera	Ref. [4]
1.77	Corn straw	Ref. [5]
1.2	Rice culms	Ref. [6]
2.07	Starch and squid ink	Ref. [7]
2.44	Waste cotton	Ref. [8]
1.4	Enteromorpha prolifera	Ref. [9]
1.089	Enteromorpha prolifera	Ref. [10]
1.42	Luffa	Ref. [11]
1.78	Chitosan	Ref. [12]
1.3	Luffa	Ref. [13]
1.3	Wood	Ref. [14]
4.1	Chitosan and cuttlefish ink	**Our work**

Table S4. Materials cost analysis of the 3 wt% CI/CS hydrogel.

Materials	Price (USD kg^{-1})	Unit cost (USD m^{-2})
Chitosan	13.9	2.91
Cuttlefish ink	49.4	5.18
Acetic acid	56.0	0.25
		Sum: 8.35

The CI/CS hydrogel evaporator was fabricated by the freeze-drying method. Therefore, the fabrication cost is mainly contributed by the materials cost, equipment usage, and electricity cost. The equipment used in this work are freeze-dryer, freezer, and stirring plate. The equipment usage and electricity cost is hard to be estimated when calculating the laboratory-scale cost. The unit price of materials and chemicals used for CI/CS hydrogel evaporator fabrication is listed in Table S4 and it can be further reduced for scalable industrial production.

Reference

[1] Gu, Yufei, et al. "Integrated photothermal aerogels with ultrahigh-performance solar steam generation." *Nano Energy* 74 (2020): 104857.

[2] Gu, Yufei, et al. "Self-Cleaning Integrative Aerogel for Stable Solar-Assisted Desalination." *Global Challenges* 5.1 (2021): 2000063.

[3] Hu, Xiaozhen, et al. "Tailoring graphene oxide-based aerogels for efficient solar steam generation under one sun." *Advanced materials* 29.5 (2017): 1604031.

[4] Yang, Lin, et al. "Sustainable biochar-based solar absorbers for high-performance solar-driven steam generation and water purification." *ACS Sustainable Chemistry & Engineering* 7.23 (2019): 19311-19320.

[5] Li, Jiyan, et al. "Ultralight biomass porous foam with aligned hierarchical channels as salt-resistant solar steam generators." *ACS applied materials & interfaces* 12.1 (2019): 798-806.

[6] Fang, Qile, et al. "Full biomass-derived solar stills for robust and stable evaporation to collect clean water from various water-bearing media." *ACS applied materials & interfaces* 11.11 (2019): 10672-10679.

[7] Xu, Yuanlu, et al. "Low cost, facile, environmentally friendly all biomass-based squid ink-starch hydrogel for efficient solar-steam generation." *Journal of Materials Chemistry A* 8.45 (2020): 24108-24116.

[8] Yu, Fang, et al. "Biomass-Derived Bilayer Solar Evaporator with Enhanced Energy Utilization for High-Efficiency Water Generation." *ACS Applied Materials & Interfaces* (2020).

[9] Yang, Lin, et al. "Marine biomass-derived composite aerogels for efficient and durable solar-driven interfacial evaporation and desalination." *Chemical Engineering Journal* (2020): 128051.

[10] Zhu, Mengmeng, et al. "Biomass Carbon Materials for Efficient Solar Steam Generation Prepared from Carbonized Enteromorpha Prolifera." *Energy Technology* 8.5 (2020): 1901215.

[11] Liu, Chao, et al. "An ‘antifouling’ porous loofah sponge with internal microchannels as solar absorbers and water pumpers for thermal desalination." *Journal of Materials Chemistry A* 8.25 (2020): 12323-12333.

[12] Irshad, Muhammad Sultan, et al. "Semiconductive, Flexible MnO2 NWs/Chitosan Hydrogels for Efficient Solar Steam Generation." *ACS Sustainable Chemistry & Engineering (2021).*

[13] Saleque, Ahmed Mortuza, et al. "Solar Driven Interfacial Steam Generation Derived from Biodegradable Luffa Sponge." *Advanced Sustainable Systems* (2021): 2000291.

[14] Song, Lian, et al. "Fe3O4/polyvinyl alcohol decorated delignified wood evaporator for continuous solar steam generation." *Desalination* 507 (2021): 115024.